Generation of optical Schrödinger cat states by generalized photon subtraction

Kan Takase, Jun-ichi Yoshikawa, Warit Asavanant, Mamoru Endo, and Akira Furusawa

Generation of optical Schrödinger's cat states by generalized photon subtraction

Kan Takase,[1] Jun-ichi Yoshikawa,[1] Warit Asavanant,[1] Mamoru Endo,[1] and Akira Furusawa[1, *]

[1]*Department of Applied Physics, School of Engineering,*
The University of Tokyo, 7-3-1 Hongo, Bunkyo-ku, Tokyo 113-8656, Japan
(Dated: November 29, 2020)

We propose a high-rate generation method of optical Schrödinger's cat states. Thus far, photon subtraction from squeezed vacuum states has been a standard method in cat-state generation, but its constraints on experimental parameters limit the generation rate. In this paper, we consider the state generation by photon number measurement in one mode of two-mode Gaussian states, which is a generalization of conventional photon subtraction, and derive the conditions to generate high-fidelity and large-amplitude cat states. Our method relaxes the constraints on experimental parameters, allowing us to optimize them and attain a high generation rate. Supposing realistic experimental conditions, the generation rate of cat states with large amplitudes ($|\alpha| \geq 2$) can exceed megacounts per second, about 10^3 to 10^6 times better than typical rates of conventional photon subtraction. This rate would be improved further by the progress of related technologies. Ability to generate non-Gaussian states at a high rate is important in quantum computing using optical continuous variables, where scalability have been demonstrated but preparation of non-Gaussian states of light remains as a challenging task for universality and fault-tolerance. Our proposal reduces the difficulty of the state preparation and opens a way for practical applications in quantum optics.

I. INTRODUCTION

Quantum computers attract attention as high-performance information processors, and implementations based on various physical systems have been extensively studied. Among these systems, an optical continuous-variable (CV) system is a promising candidate, where scalable measurement-based quantum computing can be performed on Gaussian entangled states called cluster states [1–3]. Generation of large-scale cluster states [4–6] and gate operation on them [7, 8] have been reported. For practical quantum computing, non-Gaussian states of light are essential resources because they enable universal quantum computing on cluster states in a fault-tolerant way [9–11]. Despite the importance of the non-Gaussian states, their stable supply is challenging because their high-purity generations are mainly based on heralding scheme [12], which is probabilistic. With the current technology, the computational speed of quantum computing would be strongly limited by the generation rate of non-Gaussian states not the processing platforms [7, 8]. Therefore, high-rate generation of non-Gaussian states is key for optical CV quantum computing.

Schrödinger's cat states are typical non-Gaussian states of light, which are coherent-state superpositions given by $|\alpha\rangle \pm |-\alpha\rangle$. Cat states with $|\alpha| \geq 2$ can be utilized as qubits of CV quantum computing [13, 14] or resources for quantum error correction coding [15–17]. However, even in the best experiments, the generated optical cat states have the amplitudes $1.61 \leq |\alpha| \leq 1.85$ [18–23]. This is mainly because the generation rate of the large-amplitude cat states is too low in conventional methods. A standard method of cat-state generation is the photon subtraction method shown in Fig. 1(a) [22–27]. In this method, a squeezed vacuum is fed into a beam splitter whose reflectance is set $R \ll 1$ for beam tapping. By detecting photons in the tapping channel, we obtain cat-like states

in the other output channel. To achieve $|\alpha| \geq 2$, the number of detected photons should be $n \geq 4$ [24]. Such events are quite rare because the probability to detect n photons has order R^n. Although other generation methods have also been actively studied, it is difficult to simultaneously achieve a high generation rate and a high fidelity. Methods in Refs. [19–21, 28, 29] are not suitable for high-rate generation due to either multiple conditioning processes or use of ancillary non-Gaussian states, which are generated probabilistically. Photon-number measurement in one mode of two-mode Gaussian states is a straightforward approach for a high-rate cat-state generation because it involves only one probabilistic process. Thus far, this approach has been studied in limited cases where input states contain few photons [18] and where up to three photons are measured [30]. Relaxing such constraints would be fruitful because more than a few photons should be detected to achieve a large amplitude and such events occur frequently when the input states contain many photons.

In this paper, we propose a general method of cat-state generation by photon-number measurement on two-mode Gaussian states, which we call "generalized photon subtraction

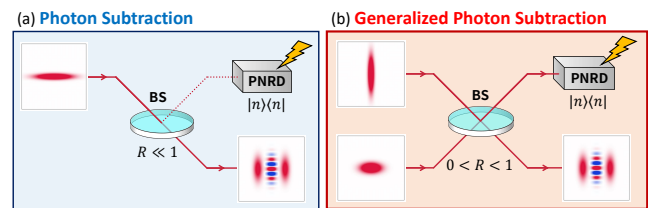(a) Photon Subtraction   (b) Generalized Photon Subtraction

FIG. 1. (a) Photon subtraction method. A weak beam is tapped by a beam splitter (BS) from a squeezed vacuum. When a photon number resolving detector (PNRD) detects photons in the tapping channel, cat-like state are heralded. (b) Generalized photon subtraction (GPS). Two squeezed vacuum states squeezed in orthogonal directions interfere at a beam splitter. Photon number measurement heralds cat-like states.

(GPS)" shown in Fig. 1(b). In GPS, we suppose detection of arbitrary number of photons in one mode of arbitrary two-mode Gaussian pure states. Then, we analytically derive conditions to generate high-fidelity and large-amplitude cat states. Describing the state generation process of GPS by wavefunctions, we probe that a wavefunction that approximates cat states well [20] can be exactly generated in a setup shown in Fig. 1(b). Such a wavufunction-based description is natural in a CV system and is in contrast to a numerical optimization in Fock basis truncated to a finite dimension, which is typically seen in Refs. [28, 30].

Supposing realistic experimental conditions, the generation rate of cat states with $|\alpha| \geq 2$ can exceed megacounts per second (Mcps), about 10^3 to 10^6 times better than typical rates of conventional photon subtraction. This rate is clearly sufficient for state verification experiments, and, furthermore, is as fast as the computational speed of recently demonstrated CV quantum information processors [7, 8]. In spite of much improvement of the generation rate, GPS utilizes only two squeezed vacuum states, one beam splitter, and one photon number resolving detector (PNRD). Thus, the implementation of GPS is within reach of the current technology. Our proposal would reduce the difficulty in the state preparation and open a way for fault-tolerant CV quantum computing.

This paper is organized as follows; basics of optical cat states are given in Sec. II A; we introduce GPS in Sec. II B, and show the way of implementation in Sec. II C; section II D is devoted to discuss the validity of the condition of cat-state generation introduced in the previous sections; comparison of the generation rate with other methods is shown in Sec. III; finally, we summarize our proposal in Sec. IV.

II. GENERALIZED PHOTON SUBTRACTION

A. Optical Schrödinger's cat states

Optical Schrödinger's cat states are often defined as superposition of coherent states with opposite phases. Coherent states are given by

$$|\alpha\rangle = \exp(\alpha \hat{a}^\dagger - \alpha^* \hat{a}) |0\rangle, \qquad (1)$$

where $\hat{a}$ and $\hat{a}^\dagger$ are annihilation and creation operators and $|0\rangle$ is a vacuum state. $\hat{a}$ and $\hat{a}^\dagger$ satisfy $[\hat{a}, \hat{a}^\dagger] = 1$. Without loss of generality, we assume $\alpha \in \mathbb{R}, \alpha > 0$ and define cat states as

$$\left|\text{Cat}_{\alpha,k}\right\rangle \equiv \frac{1}{N_{\alpha,k}} \left[|\alpha\rangle + (-1)^k |-\alpha\rangle \right], \qquad (2)$$

where $N_{\alpha,k} = \sqrt{2(1 + (-1)^k \exp(-2\alpha^2))}$. Some previous methods generate squeezed cat states $\hat{S}(r) \left|\text{Cat}_{\alpha,k}\right\rangle$ not the original cat states $\left|\text{Cat}_{\alpha,k}\right\rangle$ [18, 20, 30], where $\hat{S}(r) = \exp\left[r\left(\hat{a}^{\dagger 2} - \hat{a}^2\right)/2\right]$ $(r \in \mathbb{R})$ is a squeezing operator. The squeezing operation can reduce the average photon number of cat states, and thus the squeezed cat states survive longer than usual cat states in lossy environment [31]. If we want to use the cat states that are not squeezed, we can unsqueeze them deterministically [32].
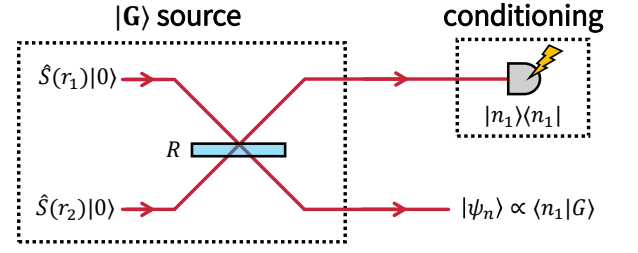

FIG. 2. Schematic of GPS. Firstly, a two-mode Gaussian state $|G\rangle$ is prepared. Detection of n photons in one mode of $|G\rangle$ heralds $|\psi_n\rangle$ in the other mode. By preparing proper $|G\rangle$, the outcome state $|\psi_n\rangle$ approximates cat states well (Sec. II B). Such $|G\rangle$ can be generated from two squeezed vacuum states and a beam splitter (Sec. II C).

We express our state generation process by wavefunctions about quadratures $\hat{x} = \left(\hat{a} + \hat{a}^\dagger\right)/\sqrt{2}$ and $\hat{p} = \left(\hat{a} - \hat{a}^\dagger\right)/\sqrt{2}i$. The quadratures satisfy a commutation relation $[\hat{x}, \hat{p}] = i$. The wavefunctions of squeezed cat states are given by

$$\left\langle x \left| \hat{S}(r) \right| \text{Cat}_{\alpha,k} \right\rangle \propto e^{-\frac{s^2}{2}\left(x - \sqrt{2}\alpha/s\right)^2} + (-1)^k e^{-\frac{s^2}{2}\left(x + \sqrt{2}\alpha/s\right)^2}, \quad (3)$$

$$\left\langle p \left| \hat{S}(r) \right| \text{Cat}_{\alpha,k} \right\rangle \propto \left(e^{-i\sqrt{2}\alpha p/s} + (-1)^k e^{i\sqrt{2}\alpha p/s} \right) e^{-\frac{1}{2s^2}p^2}, \quad (4)$$

where $|x\rangle, |p\rangle$ are the eigenstates of $\hat{x}, \hat{p}$ and $s = e^r$. The squeezing operator gives $\hat{S}^\dagger(r)\hat{x}\hat{S}(r) = \hat{x}e^{-r}$ and $\hat{S}^\dagger(r)\hat{p}\hat{S}(r) = \hat{p}e^r$, and thus $\hat{x}$ is squeezed when $r > 0$. In Ref. [20], it is shown that the function form of $x^n e^{-\kappa x^2}$ $(\kappa > 0)$ is a good approximation of the x-wavefunction of cat states with amplitude $\alpha = \sqrt{n}$ and parity $k = n$. More precisely, this approximation is given by

$$\left\langle x \left| \hat{S}(r) \right| \text{Cat}_{\sqrt{n},n} \right\rangle \approx \left\langle x \middle| \psi_{\text{approx}} \right\rangle \propto x^n e^{-\frac{s^2}{4}x^2}. \qquad (5)$$

The fidelity between $\hat{S}(r) \left|\text{Cat}_{\sqrt{n},n}\right\rangle$ and $\left|\psi_{\text{approx}}\right\rangle$ is $F_n \approx 1 - 0.03/n$ [20]. In the following, we propose a method to generate states having wavefunctions $x^n e^{-\kappa x^2}$ by detection of n photons.

B. Generalized photon subtraction

In conventional photon subtraction, a squeezed vacuum is fed into a beam splitter and photon number measurement is performed in a tapping mode to herald cat states (Fig. 1(a)). From a different perspective, the conventional photon subtraction consists of two parts: preparation of two-mode Gaussian states and non-Gaussian measurement on them. Note that in non-Gaussian state generation, either initial states or measurement should be non-Gaussian. For high-rate state generation, it is desirable that the initial states are Gaussian because we can prepare them deterministically. The conventional photon subtraction only utilizes a small subspace of arbitrary two-mode Gaussian states due to its low degree of freedom, and thus there is room to find a more efficient generation method

of cat states in a generalized situation. In this section, we consider the generation of cat states by detection of arbitrary number of photons on arbitrary two-mode Gaussian pure states, which we call generalized photon subtraction (GPS). GPS also generalizes other cat-state generation methods supposing input states with few photons [18] or up to three-photon measurement [30] in the same setup. Experimental feasibility of GPS is discussed in Sec. II C.

Firstly, we overview the process of state generation shown in Fig. 2. A two-mode Gaussian state $|G\rangle$ is expressed by a complex Gaussian function $G(x_1, x_2)$ as

$$|G\rangle = \iint dx_1 dx_2 \, G(x_1, x_2) |x_1\rangle |x_2\rangle. \quad (6)$$

When n photons are measured in the mode 1, the state $|G\rangle$ is affected as follows,

$$\langle n_1|G\rangle = \iint dx_1 dx_2 \, G(x_1, x_2) \langle n_1|x_1\rangle |x_2\rangle$$
$$= \int dx_2 \left[\int dx_1 \, G(x_1, x_2) \phi_n(x_1) \right] |x_2\rangle, \quad (7)$$

where $\phi_n(x) = \langle x|n\rangle$. Therefore, the unnormalized wavefunction of the outcome state is

$$\Psi_n(x_2) = \int dx_1 \, G(x_1, x_2) \phi_n(x_1). \quad (8)$$

Thus, the bivariate function $G(x_1, x_2)$ linearly transforms $\phi_n(x_1)$ into $\Psi_n(x_2)$. The function $\Psi_n(x_2)$ is not normalized because the conditioning process is probabilistic. The probability $P(n)$ to detect n photons and normalized wavefunction $\psi_n(x_2)$ are given by

$$P(n) = \int dx_2 \, |\Psi_n(x_2)|^2, \quad (9)$$

$$\psi_n(x_2) = \frac{1}{\sqrt{P(n)}} \Psi_n(x_2). \quad (10)$$

Secondly, let us consider the conditions imposed to $G(x_1, x_2)$ in cat-state generation. $G(x_1, x_2)$ is given by

$$G(x_1, x_2) = \frac{|\sigma|^{\frac{1}{4}}}{\sqrt{\pi}} \exp\left[-\frac{1}{2}(\boldsymbol{x} - \boldsymbol{\mu})^T \sigma (\boldsymbol{x} - \boldsymbol{\mu}) - i\boldsymbol{x}^T \boldsymbol{\nu} \right], \quad (11)$$

$$\boldsymbol{x} = \begin{pmatrix} x_1 \\ x_2 \end{pmatrix}, \, \boldsymbol{\mu} = \begin{pmatrix} \mu_1 \\ \mu_2 \end{pmatrix}, \, \boldsymbol{\nu} = \begin{pmatrix} \nu_1 \\ \nu_2 \end{pmatrix}, \, \sigma = \begin{pmatrix} \sigma_{11} & \sigma_{12} \\ \sigma_{21} & \sigma_{22} \end{pmatrix},$$

where $|M|$ denotes determinant of a matrix M. σ satisfies $\sigma = \sigma^T$ and its elements are complex numbers in general. σ becomes a real matrix when quadratures x_1, x_2 and p_1, p_2 are uncorrelated. $\boldsymbol{\mu}$ and $\boldsymbol{\nu}$ denote the displacement of $|G\rangle$ about x and p. The wavefunction of Fock state $|n\rangle$ is given by

$$\phi_n(x) = \frac{1}{\pi^{1/4} \sqrt{2^n n!}} H_n(x) \, e^{-\frac{1}{2}x^2}, \quad (12)$$

where $H_n(x)$ is a n-th order Hermite polynomial $H_n(x) = (-1)^n e^{x^2} \frac{d^n}{dx^n} e^{-x^2}$. Our target states are the cat states with $\alpha \in \mathbb{R}$, and thus $\Psi_n(x_2)$ should be an even or odd real function with non-Gaussian profile. From the symmetry $\phi_n(-x) = (-1)^n \phi_n(x)$, it is sufficient to assume the case where $\boldsymbol{\mu} = \boldsymbol{\nu} = \boldsymbol{0}$

and σ is a real positive-definite matrix. From Eq. (5), we expect $\Psi_n(x) \propto x^n e^{-\frac{s^2}{4}x^2}$. The key relation to obtain this function is given by

$$(\phi_0 * \phi_n)(x) = \frac{1}{\sqrt{2^n n!}} x^n \, e^{-\frac{1}{4}x^2}, \quad (13)$$

where $(f * g)(x)$ denotes the convolution of $f(x)$ and $g(x)$. This equation is derived from an integral formula,

$$\int_{-\infty}^{\infty} dy \, H_n(y) \, e^{-(y-x)^2} = \sqrt{\pi}(2x)^n. \quad (14)$$

We transform $G(x_1, x_2)$ so that we can use Eq. (13) in the calculation of Eq. (8),

$$G(x_1, x_2)$$
$$= \frac{|\sigma|^{\frac{1}{4}}}{\sqrt{\pi}} \exp\left[-\frac{|\sigma|}{2\sigma_{11}} x_2^2 \right] \exp\left[-\frac{1}{2}\sigma_{11} \left(x_1 + \frac{\sigma_{12}}{\sigma_{11}} x_2 \right)^2 \right]$$
$$= |\sigma|^{\frac{1}{4}} \phi_0 \left(\sqrt{\frac{|\sigma|}{\sigma_{11}}} x_2 \right) \phi_0 \left(-\sqrt{\sigma_{11}} \left(x_1 + \frac{\sigma_{12}}{\sigma_{11}} x_2 \right) \right). \quad (15)$$

We can use Eq. (13) when the following relations are satisfied,

$$\sigma_{11} = 1, \, \sigma_{12} \neq 0. \quad (16)$$

The latter condition is obvious because $\sigma_{12} = 0$ means x_1 and x_2 are independent, hence photon number measurement does not affect the state in the other mode. When Eq. (16) is satisfied, we get

$$\Psi_n(x_2) = |\sigma|^{\frac{1}{4}} \phi_0 \left(\sqrt{|\sigma|} x_2 \right) \int dx_1 \, \phi_0 (-x_1 - \sigma_{12} x_2) \phi_n(x_1)$$
$$= |\sigma|^{\frac{1}{4}} \phi_0 \left(\sqrt{|\sigma|} x_2 \right) (\phi_0 * \phi_n) (-\sigma_{12} x_2)$$
$$= \left(\frac{|\sigma|}{\pi} \right)^{\frac{1}{4}} \frac{(-\sigma_{12})^n}{\sqrt{2^n n!}} x_2^n \exp\left(-\frac{|\sigma| + \sigma_{22}}{4} x_2^2 \right). \quad (17)$$

From Eq. (5), the outcome state satisfies

$$|\psi_n\rangle \approx \hat{S}(r_c) \left| \text{Cat}_{\sqrt{n},n} \right\rangle, \, e^{2r_c} = |\sigma| + \sigma_{22}. \quad (18)$$

Therefore, the detection of n photons heralds cat-like states with the amplitude $\alpha = \sqrt{n}$. As we mentioned in Sec. II A, the fidelity of $|\psi_n\rangle$ and $\hat{S}(r_c) \left| \text{Cat}_{\sqrt{n},n} \right\rangle$ is $F_n \approx 1 - 0.03/n$ [20].

Summarizing the above, we introduced GPS as photon number measurement on arbitrary two-mode Gaussian states. In the conditions of $\sigma_{11} = 1$ and $\sigma_{12} \neq 0$, the outcome states approximate cat states well as shown in Eq. (18). The dependence of the outcome states on σ_{11} is discussed in Sec. II D.

C. Preparation of two-mode Gaussian states

We discuss preparation of the two-mode Gaussian state $|G\rangle$ and derive ones of the key results of this paper given by Eqs. (22) and (23). $|G\rangle$ is generated from the interference of two squeezed vacuum states at a beam splitter as shown in Fig. 2. When the quadratures x_1, x_2 and p_1, p_2 are uncorrelated, the matrix σ^{-1} is equal to a covariance matrix about x_1 and x_2.
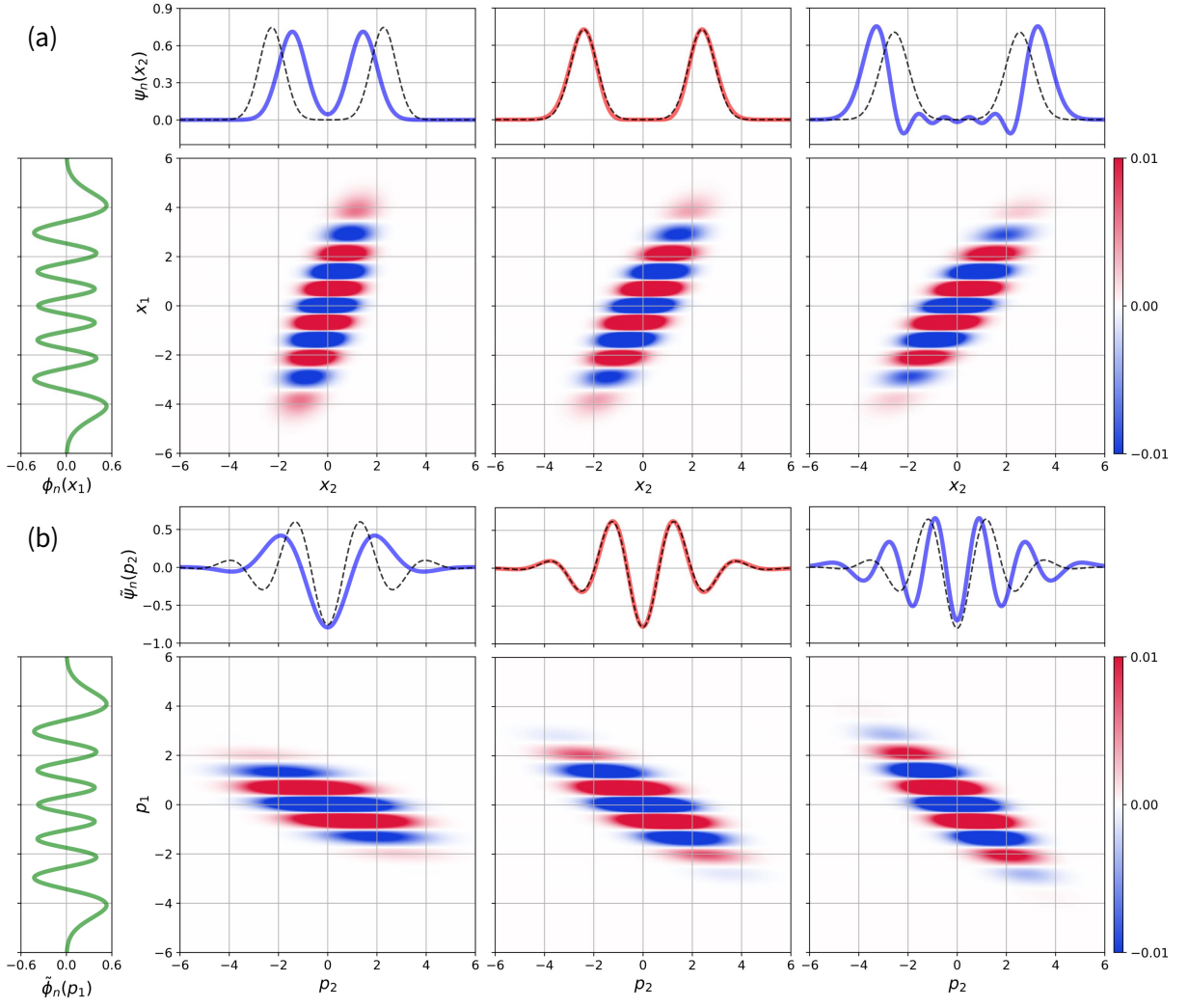
FIG. 3. (a) The plots of the functions $\phi_n(x_1)$, $\phi_n(x_1)G(x_1, x_2)$, and $\psi_n(x_2)$ in the case of $r_1 = -r_2 = 0.576$ (5 dB squeezing) and $n = 10$. From the left, $\sigma_{11} = 0.6$ ($R = 0.10$), $\sigma_{11} = 1$ ($R = 0.24$), and $\sigma_{11} = 1.4$ ($R = 0.38$). The black broken lines show the wavefunction of $\hat{S}(r_c)\left|\text{Cat}_{\sqrt{10},10}\right\rangle$ in the case of $\sigma_{11} = 1$ (see Eq. (18)). When $\sigma_{11} = 1$, the fidelity of $|\psi_n\rangle$ and the target state is $F_{10} \approx 0.997$. (b) Similar plots about p.

Thus, σ^{-1} of the initial squeezed vacuum states, which we put $\hat{S}(r_1)|0\rangle \otimes \hat{S}(r_2)|0\rangle$, is given by

$$\sigma^{-1} = \begin{pmatrix} \langle \hat{x}_1^2 \rangle & \langle \hat{x}_1 \hat{x}_2 \rangle \\ \langle \hat{x}_2 \hat{x}_1 \rangle & \langle \hat{x}_2^2 \rangle \end{pmatrix} = \begin{pmatrix} e^{-2r_1} & 0 \\ 0 & e^{-2r_2} \end{pmatrix}. \quad (19)$$

Generally, beam splitters transform $(\hat{a}_1\ \hat{a}_2)^T$ by an arbitrary unitary matrix M_{BS}. In our case, we can assume M_{BS} is a real orthogonal matrix and $\boldsymbol{x}$ is transformed to $M_{\text{BS}}\boldsymbol{x}$ because σ is a real matrix. Then, the matrix σ^{-1} is transformed to $M_{\text{BS}}\sigma^{-1}M_{\text{BS}}^T$. When the beam splitter has the power reflectance (transmittance) R ($T = 1 - R$), σ^{-1} and σ are given by

$$\sigma^{-1} = \begin{pmatrix} \sqrt{R} & \sqrt{T} \\ -\sqrt{T} & \sqrt{R} \end{pmatrix} \begin{pmatrix} e^{-2r_1} & 0 \\ 0 & e^{-2r_2} \end{pmatrix} \begin{pmatrix} \sqrt{R} & -\sqrt{T} \\ \sqrt{T} & \sqrt{R} \end{pmatrix}$$

$$= \begin{pmatrix} Re^{-2r_1} + Te^{-2r_2} & \sqrt{RT}\left(e^{-2r_2} - e^{-2r_1}\right) \\ \sqrt{RT}\left(e^{-2r_2} - e^{-2r_1}\right) & Te^{-2r_1} + Re^{-2r_2} \end{pmatrix}, \quad (20)$$

$$\sigma = \begin{pmatrix} Re^{2r_1} + Te^{2r_2} & \sqrt{RT}\left(e^{2r_1} - e^{2r_2}\right) \\ \sqrt{RT}\left(e^{2r_1} - e^{2r_2}\right) & Te^{2r_1} + Re^{2r_2} \end{pmatrix}. \quad (21)$$

Therefore, the conditions of GPS are given by

$$\sigma_{11} = Re^{2r_1} + Te^{2r_2} = 1, \quad (22)$$

$$\sigma_{12} = \sqrt{RT}\left(e^{2r_1} - e^{2r_2}\right) \neq 0. \quad (23)$$

We can prepare desired $|G\rangle$ by selecting parameters $r_1, r_2 \in \mathbb{R}$ and R ($0 \leq R \leq 1$) satisfying these conditions. If and only if $r_1 r_2 < 0$, there exists R that satisfies Eqs. (22) and (23). Thus, the initial squeezed vacuum states should be squeezed in orthogonal directions. When $\sigma_{11} = 1$, the squeezing factor of the outcome states in Eq. (18) is

$$e^{2r_c} = e^{2(r_1+r_2)} + e^{2r_1} + e^{2r_2} - 1. \quad (24)$$

Supposing $r_1 = -r_2 > 0$ and $e^{2r_1} \gg 1$, the generated cat states are as squeezed as the inputs because $e^{2r_c} \approx e^{2r_1}$.
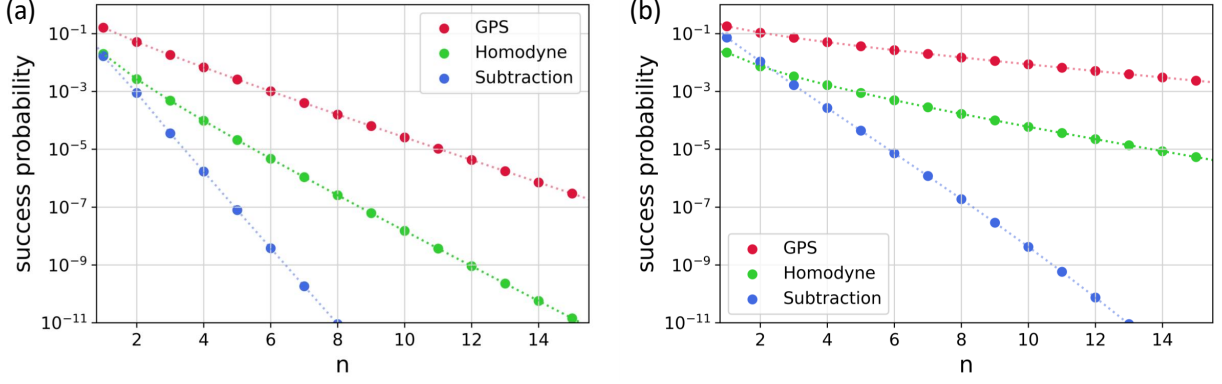
FIG. 4. (a),(b) Comparison of the success probability to generate a Schrödinger's cat state with $\alpha = \sqrt{n}$. The compared methods are GPS, the homodyne conditioning method, and conventional photon subtraction. In each method, we suppose the squeezing parameters of inputs are $|r| = 0.576$ (5 dB squeezing) in (a) and $|r| = 1.15$ (10 dB squeezing) in (b).

We briefly mention another implementation of GPS. Let us apply identity operation $\hat{I} = \hat{S}(r_2)\hat{S}^\dagger(r_2)$ to the both input states. By moving operators $\hat{S}(r_2)$ after the beam splitter, the inputs become $\hat{S}(r_1 - r_2)|0\rangle$ and $|0\rangle$. Although the inputs are the same as conventional photon subtraction, the projective measurement is generalized to $\hat{S}(r_2)|n\rangle$ and $R \ll 1$ is not assumed. These two implementation generates the same outcome states up to a squeezing operation.

D. Dependence on σ_{11}

In this section, we discuss how the parameter σ_{11} affects the outcome states and show that $\sigma_{11} = 1$ is a reasonable condition. Figure 3(a) shows the plots of the functions $\phi_n(x_1)$, $\phi_n(x_1)G(x_1, x_2)$, and $\psi_n(x_2)$ to visualize Eq. (8). From the left, each plot corresponds to $\sigma_{11} < 1$, $\sigma_{11} = 1$, and $\sigma_{11} > 1$. We can see the tilted Gaussian structures of $G(x_1, x_2)$ striped by $\phi_n(x_1)$. In Fig. 3(a), they get more tilted from x_2 axis as σ_{11} increases. When $\sigma_{11} = 1$, $\psi_n(x_2)$ has two peaks because the integral about x_1 averages out the stripe structure except for the two peaks on the both ends. $\psi_n(x_2)$ and the target cat state (black broken line) are almost identical. When $\sigma_{11} < 1$, $\psi_n(x_2)$ has a cat-like waveform but its amplitude decreases. When $\sigma_{11} > 1$, the interval of the highest peaks increases but an unwanted oscillation appears. This is because the Gaussian shape tilts too much for the stripe to cancel. Analytically, we can derive $\Psi_n(x_2)$ from Eqs. (8) and (15) as follows,

$$\Psi_n(x_2) = |\sigma|^{\frac{1}{4}} \, \phi_0\left(\sqrt{\frac{|\sigma|}{\sigma_{11}}} x_2\right) I_n^{(\sigma_{11})}\left(-\frac{\sigma_{12}}{\sigma_{11}} x_2\right), \quad (25)$$

$$I_n^{(\sigma_{11})}(x) = \int dy \, \phi_0\left(\sqrt{\sigma_{11}}(x - y)\right) \phi_n(y). \quad (26)$$

The waveform of $\psi_n(x_2)$ is mainly decided by the function $I_n^{(\sigma_{11})}(x)$. When $\sigma_{11} = 1$, $\psi_n(x_2)$ is close to the wavefunction of cat states due to the relation $I_n^{(1)}(x) = (\phi_0 * \phi_n)(x)$. When

$0 < \sigma_{11} < 1$, we can derive

$$I_n^{(\sigma_{11})}(x) = \left(g * I_n^{(1)}\right)(x), \quad g(x) = \frac{\exp\left(-\frac{\sigma_{11}}{2(1-\sigma_{11})} x^2\right)}{\sqrt{2(1 - \sigma_{11})\pi}}. \quad (27)$$

Thus, we have another Gaussian convolution on $I_n^{(1)}(x)$. In this case, we still have a cat-like wavefunction, but its effective amplitude decreases due to the extra convolution. When $\sigma_{11} > 1$, $\phi_n(x)$ is convolved by a Gaussian function narrower than $\phi_0(x)$. In this case, an unwanted oscillation remains in $\psi_n(x_2)$ because the oscillation of $\phi_n(x)$ is not averaged out completely.

Figure 3(b) shows the Fourier counterpart of the functions in Fig. 3(a), that is, $\tilde{\phi}_n(p_1)$, $\tilde{\phi}_n(p_1)\tilde{G}(p_1, p_2)$, and $\tilde{\psi}_n(p_2)$. The functions $\phi_n(x_1)$ and $\tilde{\phi}_n(p_1)$ have the same waveform because $|n\rangle$ is phase insensitive. $\tilde{G}(p_1, p_2)$ is characterized by a matrix $\tilde{\sigma}$, which is equal to σ with the sign inversion of r_1, r_2. From Eqs. (20) and (21), the covariance matrix of $|G\rangle$ about p_1, p_2 is given by

$$\tilde{\sigma}^{-1} = \begin{pmatrix} \langle \hat{p}_1^2 \rangle & \langle \hat{p}_1 \hat{p}_2 \rangle \\ \langle \hat{p}_2 \hat{p}_1 \rangle & \langle \hat{p}_2^2 \rangle \end{pmatrix} = \begin{pmatrix} \sigma_{11} & -\sigma_{12} \\ -\sigma_{21} & \sigma_{22} \end{pmatrix}. \quad (28)$$

From Eq. (4), $\tilde{\psi}_n(p_2)$ should have cosine (or sine) oscillations with a Gaussian envelope. Wentzel-Kramers-Brillouin approximation [33] shows $\tilde{\phi}_n(p_1)$ has cosine (or sine) oscillations when p_1 is small. In GPS, these oscillations of $\tilde{\phi}_n(p_1)$ are mapped to $\tilde{\psi}_n(p_2)$ by a Gaussian function $\tilde{G}(p_1, p_2)$. A wider range of $\tilde{\phi}_n(p_1)$ structure appears in $\tilde{\psi}_n(p_2)$ as the variance of $|G\rangle$ about p_1 increases. Thus, $\langle \hat{p}_1^2 \rangle = \sigma_{11}$ has a critical effect on the waveform of $\tilde{\psi}_n(p_2)$. When $\sigma_{11} = 1$, $\tilde{\psi}_n(p_2)$ well approximates the ideal line. When $\sigma_{11} < 1$, smaller number of cosine oscillations appear in $\tilde{\psi}_n(p_2)$. That means the amplitude of the generated cat state gets smaller. When $\sigma_{11} > 1$, both ends of the $\tilde{\phi}_n(p_1)$ structure moves the generated state away from ideal cat states.

Like the above, the two distinct areas of the wavefunction of $|n\rangle$, two peaks and cosinusoidal oscillations, appear in $\psi_n(x_2)$ and $\tilde{\psi}_n(p_2)$ through the Gaussian functions $G(x_1, x_2)$

and $\tilde{G}(p_1, p_2)$, respectively. Supposing $\sigma_{11} = 1$, we can ensure that high-fidelity and large-amplitude cat states are generated.

III. EVALUATION OF GENERATION RATE

GPS can generate cat states at a much better rate than conventional methods. From Eqs. (9) and (17), the probability to obtain $|\psi_n\rangle$ in the condition $\sigma_{11} = 1$ is

$$P(n) = \frac{\sqrt{|\sigma|}(2n)!(\sigma_{12})^{2n}}{8^n(n!)^2}\left(\frac{|\sigma| + \sigma_{22}}{2}\right)^{-n-\frac{1}{2}}. \qquad (29)$$

GPS contains some previous works as special cases due to its generality. In these works, $P(n)$ was quite low because $|\sigma_{12}| = \sqrt{RT}\left|e^{2r_1} - e^{2r_2}\right| \ll 1$ is assumed. For example, conventional photon subtraction assumes $R \ll 1$ and $r_2 = 0$. The weak tapping condition $R \ll 1$ makes it difficult to detect photons in the tapped mode. In another example [18], two squeezed vacuum states are utilized but the low input power condition $r_1 = -r_2 \ll 1$ is assumed. Now, we have a generalized condition for cat-state generation $\sigma_{11} = 1$, so that we can select parameters that avoid undesirable conditions like $R \ll 1$ or $|r_1 - r_2| \ll 1$. In addition, GPS performs conditioning only once, and thus it is better than methods that perform conditioning more than once [20, 21, 28, 29]. Those factors indicate the potential of GPS for improvement of the state generation rate.

We compare the cat-state generation rate of GPS with the homodyne conditioning method [20] and conventional photon subtraction. In GPS, we assume $r_1 = -r_2 > 0$ and select R that satisfies $\sigma_{11} = 1$. In the homodyne conditioning method, a Fock state $|n\rangle$ is generated from a two-mode squeezed vacuum state and n photon detection, followed by 50:50 beam splitting and homodyne conditioning in one mode. When we use squeezed vacuums $\hat{S}(r)|0\rangle$ as inputs and generate cat states with fidelity about 0.99, the success probability of n photon detection and homodyne conditioning are $(1 - \tanh^2 r)\tanh^{2n} r$ and $1/(10n)$, respectively. In conventional photon subtraction, we assume $R = 0.05$ and numerically calculate the success probability in a subspace up to 50 photons by a Python library for photonic quantum computing [34, 35].

Figures 4(a) and 4(b) are the success probability to generate the cat states $\left|\text{Cat}_{\sqrt{n},n}\right\rangle$ with squeezing. We assume that the squeezing parameters of inputs are $|r| = 0.576$ (5 dB squeezing) in Fig. 4(a), and $|r| = 1.15$ (10 dB squeezing) in Fig. 4(b) in each method. In the both cases, GPS has the highest success probability, and the superiority increases as n increases. Especially, the improvement over conventional photon subtraction is remarkable. The improvement of the success rate easily reaches several orders as n increases. GPS is also better than the homodyne conditioning method by multiple orders. In this case, the difference of success rates mainly comes from the number of conditioning. The success rate to generate a cat state in GPS and the rate to generate a Fock state in the homodyne conditioning method are comparable, but the need of one more conditioning process in the latter method than the former one lowers the total success rate.
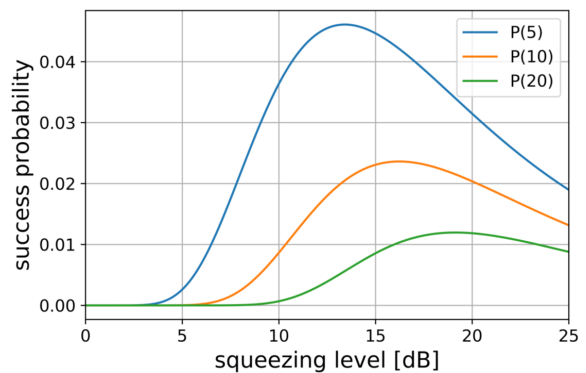

FIG. 5. The probability to detect 5, 10, and 20 photons in GPS in the case of $r_1 = -r_2$ and $\sigma_{11} = 1$.

We show a generation rate estimation of GPS. The cat states with $\alpha \geq 2$ are desired in quantum computing [14]. Thus, we are interested in the case of $n \geq 4$. Figure 5 is the behaviors of $P(5)$, $P(10)$, and $P(20)$ against the input squeezing level on the assumption of $r_1 = -r_2$ and $\sigma_{11} = 1$. We see they have each maximum value at some points. This is because the distribution of $P(n)$ gradually becomes flat as the squeezing level increases in the condition of $\sum P(n) = 1$. Thus far, $r = 1.73$ (15 dB squeezing) has been demonstrated [36]. Supposing $r_1 = -r_2 = 1.73$, we get $P(10) = 0.023$. The generation rate of $|\psi_{10}\rangle$ becomes $0.023 \times f_{\text{rep}}$ by operating the system at a rate f_{rep}. The performances of squeezed vacuum sources and PNRDs decide the limit of f_{rep}. Recent works argue that implementation of PNRDs by multiplexed on-off detectors is demanding [37, 38], and thus other methods like transition edge sensors or superconducting nanowire detectors are desired [39–43]. Because the experimental results so far [43, 44] indicate that $f_{\text{rep}} = 100$ MHz is possible, we have enough chance to generate $|\psi_{10}\rangle$ at Mcps order. Refining the performances of squeezed vacuum sources and PNRDs leads to the further improvement of this rate. Since current optical CV information processors work at MHz order [7], single cat-state source of GPS might be enough to feed cat states into the processor as inputs. This rate is 10^3 to 10^6 times better than conventional photon subtraction where we assume $0.02 \leq R \leq 0.05$ as a typical condition. Like the above, GPS would lead to generation of the large-amplitude cat states at the rate enough for implementation of quantum optical applications.

Finally, we briefly discuss the effect of photon loss, a main source of experimental imperfections. Photon losses can independently occur at input and output modes of the beam splitter. Supposing the input modes have the same degree of loss, input loss can be put together with the output loss because input loss commutes with the beam splitter. This situation is recognized that mixed states are heralded by a PNRD with a quantum efficiency $\eta < 1$ and the heralded states propagate through a damping channel. Imperfection of PNRDs and damping channel affect the generated states differently. Such effects can be analyzed by methods proposed in Refs.

[45–47]. These imperfections should be minimized to protect the non-classical features of non-Gaussian states. Thus far, PNRDs with high quantum efficiency ($\eta \geq 0.95$) have been reported [39, 40]. The effect of damping channel is usually smaller for quantum states with fewer photons. Thus, squeezed cat states, which are generated by GPS, is more robust to loss than the usual cat states [31].

IV. CONCLUSION

We have proposed GPS for a high-rate generation of optical Schrödinger's cat states. We started from a generalized situation of photon number measurement on a arbitrary two-mode Gaussian pure state, and analytically derived the conditions of cat-state generation given by Eqs. (22) and (23). Our method relaxes the constraints on experimental parameters compared to conventional methods, allowing us to select optimal parameters and improve the generation rate by multiple orders. Supposing realistic experimental conditions, the generation rate of the large-amplitude cat states ($\alpha \geq 2$) is expected to reach Mcps order, which is as fast as the system clock of current CV quantum information processors. Because the performance of GPS is limited by light sources and PNRDs, the generation rate would be much faster than Mcps order by the progress of these factors. GPS is feasible in free space thanks to its simple setup. Each component of GPS has been implemented on a chip [48–51], and thus the integration of our cat-state sources would be possible in the future. Recent breakthroughs have opened a way for scalable quantum computing on CV cluster states, but high-rate supply of non-Gaussian states remains as a challenging task for universality and fault-tolerance. Our method would reduce the difficulties in the state generation system remarkably, and make a significant progress toward optical CV quantum computing.

V. ACKNOWLEDGEMENTS

[1] R. Raussendorf, D. E. Browne, and H. J. Briegel, *Measurement-based quantum computation on cluster states*, Phys. Rev. A **68**, 022312 (2003).

[2] N. C. Menicucci, P. van Loock, M. Gu, C. Weedbrook, T. C. Ralph, and M. A. Nielsen, *Universal quantum computation with continuous-variable cluster state*, Phys. Rev. Lett. **97**, 110501 (2006).

[3] N. C. Menicucci, *Fault-tolerant measurement-based quantum computing with continuous-variable cluster states*, Phys. Rev. Lett. **112**, 120504 (2014).

[4] S. Yokoyama, R. Ukai, S. C. Armstrong, C. Sornphiphatphong, T. Kaji, S. Suzuki, J. Yoshikawa, H. Yonezawa, N. C. Menicucci, and A. Furusawa, *Ultra-large-scale continuous-variable cluster states multiplexed in the time domain*, Nature Photonics **7**, 982 (2013).

[5] M. V. Larsen, X. Guo, C. R. Breum, J. S. Neergaard-Nielsen, and U. L. Andersen, *Deterministic generation of a two-dimensional cluster state*, Science **366**, 369 (2019).

[6] W. Asavanant *et al.*, *Generation of time-domain-multiplexed two-dimensional cluster state*, Science **366**, 373 (2019).

[7] W. Asavanant *et al.*, *One-hundred step measurement-based quantum computation multiplexed in the time domain with 25 MHz clock frequency*, arXiv e-prints p. arXiv:2006.11537 (2020).

[8] M. V. Larsen, X. Guo, C. R. Breum, J. S. Neergaard-Nielsen, and U. L. Andersen, *Deterministic multi-mode gates on a scalable photonic quantum computing platform*, arXiv e-prints p. arXiv:2010.14422 (2020).

[9] S. Lloyd and S. L. Braunstein, *Quantum computation over continuous variables*, Phys. Rev. Lett. **82**, 1784 (1999).

[10] D. Gottesman, A. Kitaev, and J. Preskill, *Encoding a qubit in an oscillator*, Phys. Rev. A **64**, 012310 (2001).

[11] M. Ohliger, K. Kieling, and J. Eisert, *Limitations of quantum computing with gaussian cluster states*, Phys. Rev. A **82**, 042336 (2010).

[12] A. I. Lvovsky, P. Grangier, A. Ourjoumtsev, V. Parigi, M. Sasaki, and R. T. Tualle-Brouri, *Production and application of non-Gaussian quantum states of light*, arXiv e-prints p. arXiv:2006.16985 (2020).

[13] P. T. Cochrane, G. J. Milburn, and W. J. Munro, *Macroscopically distinct quantum-superposition states as a bosonic code for amplitude damping*, Phys. Rev. A **59**, 2631 (1999).

[14] T. C. Ralph, A. Gilchrist, G. J. Milburn, W. J. Munro, and S. Glancy, *Quantum computation with optical coherent states*, Phys. Rev. A **68**, 042319 (2003).

[15] H. M. Vasconcelos, L. Sanz, and S. Glancy, *All-optical generation of states for "encoding a qubit in an oscillator"*, Opt. Lett. **35**, 3261 (2010).

[16] D. J. Weigand and B. M. Terhal, *Generating grid states from Schrödinger-cat states without postselection*, Phys. Rev. A **97**, 022341 (2018).

[17] J. Hastrup, J. S. Neergaard-Nielsen, and U. L. Andersen, *Deterministic generation of a four-component optical cat state*, Opt. Lett. **45**, 640 (2020).

[18] K. Huang *et al.*, *Optical synthesis of large-amplitude squeezed coherent-state superpositions with minimal resources*, Phys. Rev. Lett. **115**, 023602 (2015).

[19] D. V. Sychev, A. E. Ulanov, A. A. Pushkina, M. W. Richards, I. A. Fedorov, and A. I. Lvovsky, *Enlargement of optical Schrödinger's cat states*, Nat. Photonics **11**, 379-382 (2017).

[20] A. Ourjoumtsev, H. Jeong, R. Tualle-Brouri, and P. Grangier, *Generation of optical Schrödinger cats from photon number states*, Nature **448**, 784 (2007).

[21] A. E. Ulanov, I. A. Fedorov, D. Sychev, P. Grangier, and A. I. Lvovsky, *Loss-tolerant state engineering for quantum-*

enhanced metrology via the reverse hong-ou-mandel effect, Nature Communications **7**, 11925 (2016).

[22] T. Gerrits, S. Glancy, T. S. Clement, B. Calkins, A. E. Lita, A. J. Miller, A. L. Migdall, S. W. Nam, R. P. Mirin, and E. Knill, *Generation of optical coherent-state superpositions by number-resolved photon subtraction from the squeezed vacuum*, Phys. Rev. A **82**, 031802 (2010).

[23] H. Takahashi, K. Wakui, S. Suzuki, M. Takeoka, K. Hayasaka, A. Furusawa, and M. Sasaki, *Generation of large-amplitude coherent-state superposition via ancilla-assisted photon subtraction*, Phys. Rev. Lett. **101**, 233605 (2008).

[24] M. Dakna, T. Anhut, T. Opatrný, L. Knöll, and D. G. Welsch, *Generating Schrödinger-cat-like states by means of conditional measurements on a beam splitter*, Phys. Rev. A **55**, 3184 (1997).

[25] A. Ourjoumtsev, R. Tualle-Brouri, J. Laurat, and P. Grangier, *Generating optical Schrödinger kittens for quantum information processing*, Science **312**, 83 (2006).

[26] J. S. Neergaard-Nielsen, B. M. Nielsen, C. Hettich, K. Mølmer, and E. S. Polzik, *Generation of a superposition of odd photon number states for quantum information networks*, Phys. Rev. Lett. **97**, 083604 (2006).

[27] K. Wakui, H. Takahashi, A. Furusawa, and M. Sasaki, *Photon subtracted squeezed states generated with periodically poled KTiOPO$_4$*, Opt. Express **15**, 3568 (2007).

[28] M. Eaton, R. Nehra, and O. Pfister, *Non-Gaussian and Gottesman-Kitaev-Preskill state preparation by photon catalysis*, New J. Phys. **21**, 113034 (2019).

[29] G. S. Thekkadash, B. A. Bell, I. A. Walmsley, and A. I. Lvovsky, *Engineering Schrödinger cat states with a photonic even-parity detector*, Quantum **4**, 239 (2020).

[30] D. Su, C. R. Myers, and K. K. Sabapathy, *Conversion of Gaussian states to non-Gaussian states using photon-number-resolving detectors*, Phys. Rev. A **100**, 052301 (2019).

[31] H. L. Jeannic, A. Cavaillès, K. Huang, R. Filip, and J. Laurat, *Slowing quantum decoherence by squeezing in phase space*, Phys. Rev. Lett. **120**, 073603 (2018).

[32] Y. Miwa, J. Yoshikawa, N. Iwata, M. Endo, P. Marek, R. Filip, P. van Loock, and A. Furusawa, *Exploring a new regime for processing optical qubits: Squeezing and unsqueezing single photons*, Phys. Rev. Lett. **113**, 013601 (2014).

[33] W. P. Schleich, *Quantum Optics in Phase Space*, John Wiley & Sons, Ltd (2005).

[34] N. Killoran, J. Izaac, N. Quesada, V. Bergholm, M. Amy, and C. Weedbrook, *Strawberry Fields: A Software Platform for Photonic Quantum Computing*, Quantum **3**, 129 (2019).

[35] T. R. Bromley, J. M. Arrazola, S. Jahangiri, J. Izaac, N. Quesada, A. D. Gran, M. Schuld, J. Swinarton, Z. Zabaneh, and N. Killoran, *Applications of near-term photonic quantum computers: software and algorithms*, Quantum Science and Technology **5**, 034010 (2020).

[36] H. Vahlbruch, M. Mehmet, K. Danzmann, and R. Schnabel, *Detection of 15 db squeezed states of light and their application for the absolute calibration of photoelectric quantum efficiency*, Phys. Rev. Lett. **117**, 110801 (2016).

[37] M. Jönsson and G. Björk, *Evaluating the performance of photon-number-resolving detectors*, Phys. Rev. A **99**, 043822 (2019).

[38] J. Provazník, L. Lachman, R. Filip, and P. Marek, *Benchmarking photon number resolving detectors*, Opt. Express **28**, 14839 (2020).

[39] D. Fukuda *et al.*, *Titanium-based transition-edge photon number resolving detector with 98% detection efficiency with index-matched small-gap fiber coupling*, Opt. Express **19**, 870 (2011).

[40] A. E. Lita, A. J. Miller, and S. W. Nam, *Counting near-infrared single-photons with 95% efficiency*, Opt. Express **16**, 3032 (2008).

[41] R. Nehra, A. Win, M. Eaton, R. Shahrokhshahi, N. Sridhar, T. Gerrits, A. Lita, S. W. Nam, and O. Pfister, *State-independent quantum state tomography by photon-number-resolving measurements*, Optica **6**, 1356 (2019).

[42] N. Sridhar, R. Shahrokhshahi, A. J. Miller, B. Calkins, T. Gerrits, A. Lita, S. W. Nam, and O. Pfister, *Direct measurement of the wigner function by photon-number-resolving detection*, J. Opt. Soc. Am. B **31**, B34 (2014).

[43] C. Cahall, K. L. Nicolich, N. T. Islam, G. P. Lafyatis, A. J. Miller, D. J. Gauthier, and J. Kim, *Multi-photon detection using a conventional superconducting nanowire single-photon detector*, Optica **4**, 1534 (2017).

[44] N. Takanashi, W. Inokuchi, T. Serikawa, and A. Furusawa, *Generation and measurement of a squeezed vacuum up to 100 MHz at 1550 nm with a semi-monolithic optical parametric oscillator designed towards direct coupling with waveguide modules*, Opt. Express **27**, 18900 (2019).

[45] C. N. Gagatsos, and S. Guha, *Efficient representation of Gaussian states for multimode non-Gaussian quantum state engineering via subtraction of arbitrary number of photons*, Phys. Rev. A **99**, 053816 (2019).

[46] M. Walschaers, V. Parigi, and N. Treps, *Practical Framework for Conditional Non-Gaussian Quantum State Preparation*, PRX Quantum **1**, 020305 (2020).

[47] N. Quesada, L. G. Helt, J. Izaac, J. M. Arrazola, R. Shahrokhshahi, C. R. Myers, and K. K. Sabapathy, *Simulating realistic non-Gaussian state preparation*, Phys. Rev. A **100**, 022341 (2019).

[48] T. Kashiwazaki, N. Takanashi, T. Yamashima, T. Kazama, K. Enbutsu, R. Kasahara, T. Umeki, and A. Furusawa, *Continuous-wave 6-db-squeezed light with 2.5-THz-bandwidth from single-mode ppln waveguide*, APL Photonics **5**, 036104 (2020).

[49] N. Montaut, L. Sansoni, E. Meyer-Scott, R. Ricken, V. Quiring, H. Herrmann, and C. Silberhorn, *High-efficiency plug-and-play source of heralded single photons*, Phys. Rev. Applied **8**, 024021 (2017).

[50] G. Masada, K. Miyata, A. Politi, T. Hashimoto, J. L. O'Brien, and A. Furusawa, *Continuous-variable entanglement on a chip*, Nature Photonics **9**, 316 (2015).

[51] F. Lenzini *et al.*, *Integrated photonic platform for quantum information with continuous variables*, Sci Adv **4**, eaat9331 (2018).